J. Fluid Mech. (2011), *vol.* 673, *pp.* 218–244. © Cambridge University Press 2011
doi:10.1017/S0022112010006336

Experimental measurement of large-scale three-dimensional structures in a turbulent boundary layer. Part 2. Long structures

DAVID J. C. DENNIS† AND TIMOTHY B. NICKELS

Department of Engineering, Cambridge University, Trumpington Street, Cambridge CB2 1PZ, UK

(Received 8 April 2010; revised 27 September 2010; accepted 3 December 2010;
first published online 14 March 2011)

Three-dimensional (3D) measurements of a turbulent boundary layer have been made using high-speed particle image velocimetry (PIV) coupled with Taylor's hypothesis, with the objective of characterising the very long streamwise structures that have been observed previously. The measurements show the 3D character of both low- and high-speed structures over very long volumes. The statistics of these structures are considered, as is their relationship to the important turbulence quantities. In particular, the length of the structures and their wall-normal extent have been considered and their relationship to the other components of the velocity fluctuations and the instantaneous stress.

Key words: boundary layers, boundary layer structure, turbulent boundary layers

1. Introduction

A structural element of wall-bounded turbulent flow that has recently received much attention is the, 'regime of very long meandering positive and negative streamwise velocity fluctuations', as described in Hutchins & Marusic (2007*a*). Figure 1, from Hutchins & Marusic (2007*a*), shows a sample of data from a hot-wire rake positioned at $y/\delta = 0.15$ in an $Re_\tau = 14\,380$ boundary-layer flow. A very long feature can be seen meandering through the boundary layer for over 20δ (over 6.5 m at the experimental Reynolds number). This is compared with the particle image velocimetry (PIV) result shown in the inset (*b*) in figure 1, which is said to represent a snapshot of the much longer structure, (*a*). The meandering nature of this structure is said to be the reason why its true length is not apparent in one-dimensional (1D) correlations and spectra, an explanation that is quite plausible. However, spanwise hot-wire rake measurements and the PIV measurements only give a two-dimensional (2D) 'slice' of these long structures, whereas the full 3D information is lacking.

As well as being found in the log and lower wake regions of the turbulent boundary layer, these features are also found in pipe and channel flow (Kim & Adrian 1999; Monty *et al.* 2007). It is also not only hot-wire rake measurements that have been used to detect long structures. They have been found during other PIV experiments (Ganapathisubramani, Clemens & Dolling 2006) and in direct numerical simulations (DNS; Ringuette, Wu & Pino Martin 2008). Long structures found using these techniques give weight to the idea that some kind of long structures do exist but

† Email address for correspondence: djcd2@cam.ac.uk

https://doi.org/10.1017/S0022112010006336 Published online by Cambridge University Press

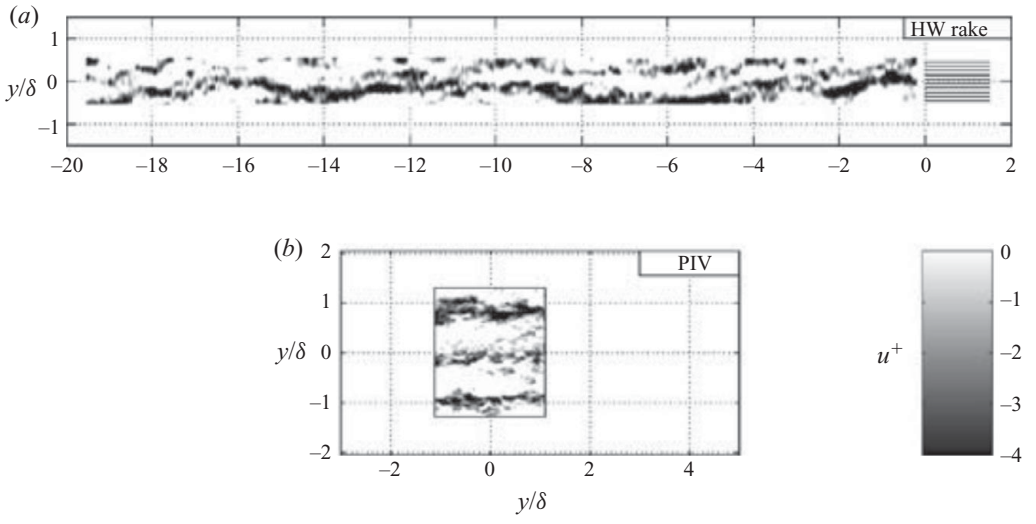


FIGURE 1. (*a*) Example rake signal at $y/\delta = 0.15$ for $Re_\tau = 14\,380$ and (*b*) PIV snapshot from Hutchins & Marusic (2007*a*). Note their y is our z.

do not give much detailed information as to their 3D nature (although Ringuette *et al.* 2008 provide some information). Structures have been found to span the whole streamwise extent of the velocity fields produced. However, PIV experiments have been restricted to a limited spatial region due to the constraints of the field of view of the camera and the difficulty in producing extensive light sheets. The largest possible streamwise extent of simultaneous measurement has so far been much less than the 20δ over which these structures are said to exist. Some aspects of long structures that have proved to be of interest are the proportion of the Reynolds shear stress they contain, which is found to be substantial (Ganapathisubramani, Longmire & Marusic 2003; Guala, Hommema & Adrian 2006), and their influence on the near-wall motions (Abe, Kawamura & Choi 2004; Hutchins & Marusic 2007*b*). The situation is similar with regard to DNS, although it is not the physical constraints of the equipment, but the processing costs of such a large domain size that have been prohibitive. There has also been a great deal of research regarding the relationship between long structures and hairpin vortex packets, see Adrian (2007) for an excellent review of these interesting aspects. In this paper, the 3D nature of these long structures is studied by constructing fully 3D velocity fields of a turbulent boundary using high-speed stereoscopic PIV in a spanwise/wall-normal plane of the flow, and then applying Taylor's hypothesis in order to convert the temporal measurements into spatial measurements. In Dennis & Nickels (2011), shorter packet-like structures were considered. In this paper, the focus will be on the long structures as discussed in the Introduction.

2. Experiment and methods

The experimental method is the same as that described in Dennis & Nickels (2011) but is repeated here for completeness. The experiments were conducted using a high-speed stereoscopic PIV system in the Cambridge University Engineering Department's turbulent boundary-layer water tunnel research facility. This unique facility has a $0.9\,\mathrm{m} \times 0.5\,\mathrm{m} \times 8\,\mathrm{m}$ long working section, and has been specially designed to produce thick turbulent boundary layers. The water is pumped through the tunnel by two

https://doi.org/10.1017/S0022112010006336 Published online by Cambridge University Press

pumps. The system is closed, and the water returns to the inlet from the outlet by way of two pipes that run underneath the working section. Before entering the working section, the water travels through a settling chamber with a 40 % perforated plate, then a 6 mm diameter honeycomb followed by a screen, then a 3 mm diameter honeycomb and finally through another two screens. There is also a 3:1 contraction. The flow is tripped at the inlet to the tunnel by a 5 mm glass rod trip, and the measurement area is 4.5 m downstream. At this location, the boundary-layer thickness is approximately $\delta = 90$ mm, the free stream velocity is $U_\infty = 0.7\,\mathrm{m\,s^{-1}}$ and the Reynolds number based on momentum thickness is $Re_\theta = 4700$ ($Re_\tau = 2460$). The turbulence intensity in the free stream (measured using laser doppler anemometry) is 0.7 %.

2.1. *Equipment*

The laser used for these experiments was a New Wave Pegasus-PIV laser. This is a dual-head, high repetition rate, diode-pumped Nd:YLF laser, with a wavelength of 527 nm, 10 mJ of energy per cavity, pulse duration of 180 ns at 1000 Hz and a beam diameter of 1.5 mm. A double-concave cylindrical lens with a focal length of −10 mm was used to expand the laser beam into a sheet. The cameras used were LaVision High Speed Star 4 digital high-speed CMOS cameras with a resolution of 1024 pixel × 1024 pixel, digital resolution (bit depth) of 12 bit and a pixel size of 17 μm × 17 μm. These were used with Scheimpflug adaptors to compensate for the oblique viewing angle and 50 mm Nikon lenses.

The seeding used was Dantec Dynamics S-HGS silver-coated hollow glass spheres with a mean diameter of 10 μm (diameter range of 2–20 μm). These are borosilicate glass particles with a spherical shape, smooth surface and thin silver coating to increase reflectivity. They are specifically designed for liquid flows as they are close to neutrally buoyant in water, having a specific gravity of 1.4.

2.2. *Experimental set-up*

A schematic of the experimental set-up is shown in figure 2. It is a sterescopic PIV set-up and therefore involves two cameras. The cameras are positioned at 45° to the measurement plane and 45° to the tunnel wall.

A prism is positioned flush against the tunnel wall so the cameras view the measurement area through the 45° face of the prism, thus eliminating the refraction of the light through the water–perspex–air interface. The laser is positioned below the tunnel, and the beam is expanded through the cylindrical lens onto a mirror and reflected vertically upwards through the floor of the tunnel.

A major feature of the experimental set-up is the orientation of the light sheet. The light sheet is perpendicular to the flow direction. The reason for this orientation is that structures in the flow will be advected through the measurement plane, and therefore 3D flow structures can be reconstructed from the measurements. This technique was used by Van Doorne (2004), to take stereoscopic PIV measurements in a pipe flow, with some success. It has also been used to examine the small-scale features of a turbulent jet flow by Ganapathisubramani, Lakshminarasimhan & Clemens (2008). The calibration was conducted using a two-level calibration plate (LaVision Type 20) with one camera viewing either side of the plate. The dewarping was done using a third-order polynomial. It was clear from the sum of the two images that the dewarping was accurate as the calibration plate dots (for the appropriate level) were coincident (i.e. they appeared as a single dot in the summed image). The average deviation of the marked locations was estimated to be 0.162 pixel.

https://doi.org/10.1017/S0022112010006336 Published online by Cambridge University Press

FOV	113 mm × 129 mm (y, z)
Initial interrogation area (IA) size	64 pixel × 64 pixel
Final IA size	32 pixel × 32 pixel
IA overlap	50 %
Resolution (x,y,z)	3.0 mm ($82\nu/U_\tau$)
Time between pulses (Δt)	1000 µs
Vector fields per second	400

TABLE 1. Fundamental quantities for the measurements using the current set up.

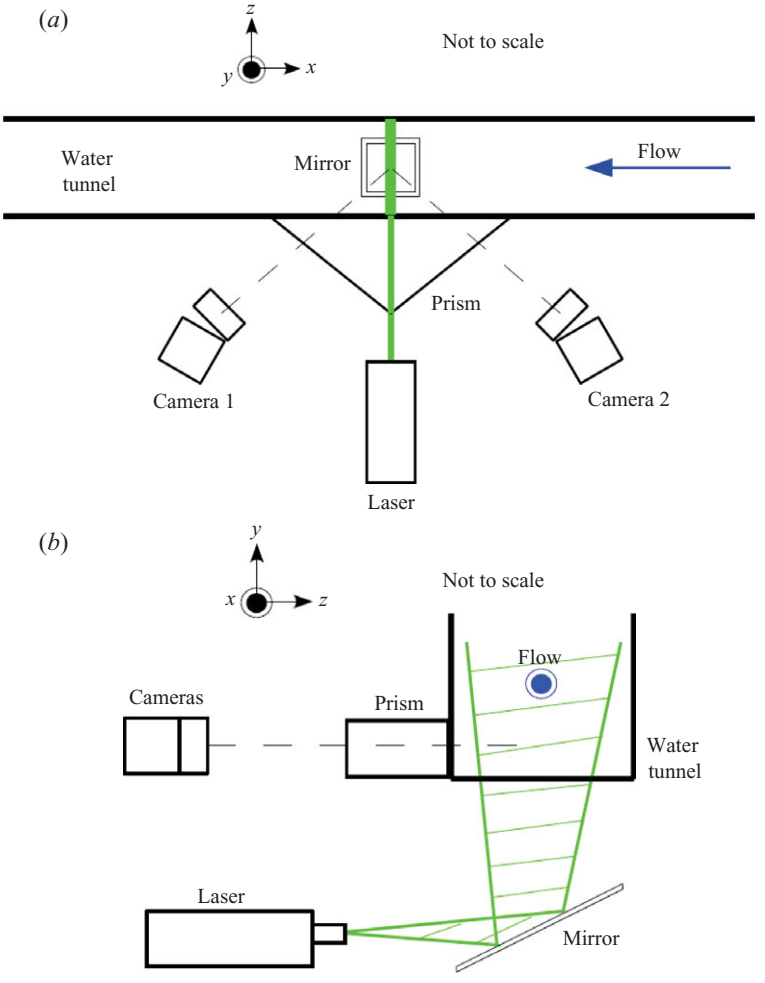


FIGURE 2. (Colour online available at journals.cambridge.org/FLM) Schematic of the cross-stream stereoscopic experimental set-up. (*a*) Top view. (*b*) Side view.

The fundamental quantities for the measurements using this set-up are stated in table 1.

2.3. *The experimental boundary layer*

The following presents some of the flow statistics obtained from the Cambridge University Engineering Department (CUED) water tunnel. The plots compare the

https://doi.org/10.1017/S0022112010006336 Published online by Cambridge University Press

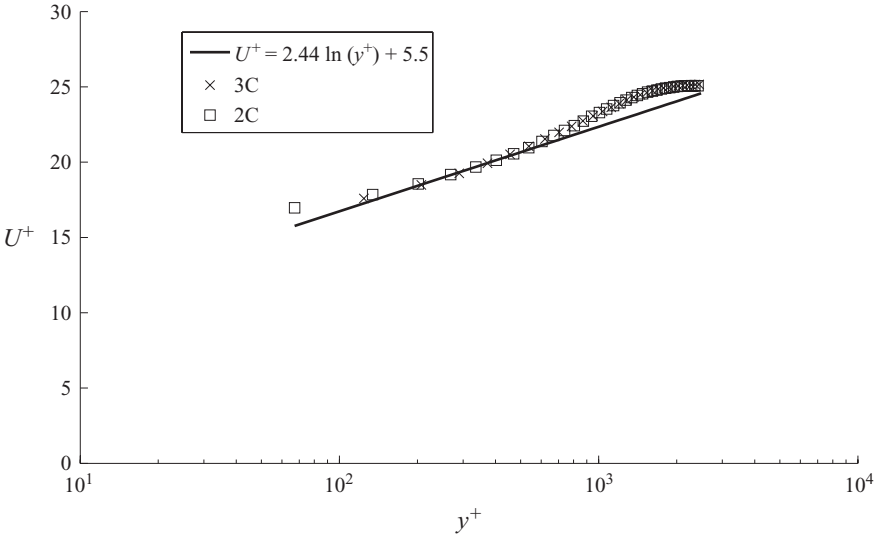


FIGURE 3. Log-law mean velocity comparison for 2C and 3C experiments.

results from a standard 2D single-camera streamwise/wall-normal 2C set-up and the cross-stream stereo 3C set-up (described in § 2.2), and in some cases a few data points from Spalart (1988) at $Re_\theta = 1410$ have also been included. It should be noted that although the Reynolds number of the Spalart (1988) data is different from the case presented here, the Reynolds stresses in the outer part of the boundary layer are fairly insensitive to the Reynolds number. Comparisons have been made with other data in the outer part and the stresses are only slightly different. The purpose of this comparison is to show that the boundary layer in the CUED water tunnel is representative of a normal turbulent boundary layer, and also to demonstrate that the statistics obtained from the cross-stream 3C experiment are similar to those obtained from the relatively simple 2C experiment, and thus to show that the stereo-3C technique has adequately captured the turbulent boundary layer. The following flow statistics were obtained from ensemble averaging 10 240 instantaneous realisations in the 3C case and 2048 in the 2C case.

Figure 3 shows the mean streamwise velocity profile in the traditional log-law form. The inner-variable scales were determined by estimating the friction velocity (u_τ) using the Clauser chart method (Clauser 1956). Since this is just a comparative test, the accuracy of the Clauser chart method is not important. Figure 3 also demonstrates that only the upper end of the log-region has been captured by the present results. This is due to the main interest being large-scale structures in the outer region of the boundary layer, which require a large field of view, and thus sacrifice high resolution near the wall. The data from the 2C and 3C experiments match well.

The root-mean-square (r.m.s.) streamwise velocity is scaled with u_τ and plotted against y/δ in figure 4. The 3C and 2C results are plotted along with some points from Spalart (1988). The data agree reasonably well with what is expected. However, it is apparent that the r.m.s. velocity is generally slightly underestimated. This is thought to be because of the moderate spatial resolution of the results in this experiment which are not capturing the smallest scales of motion. The discrepancy is particularly noticeable near the wall, where the problem of the small scales is most

https://doi.org/10.1017/S0022112010006336 Published online by Cambridge University Press

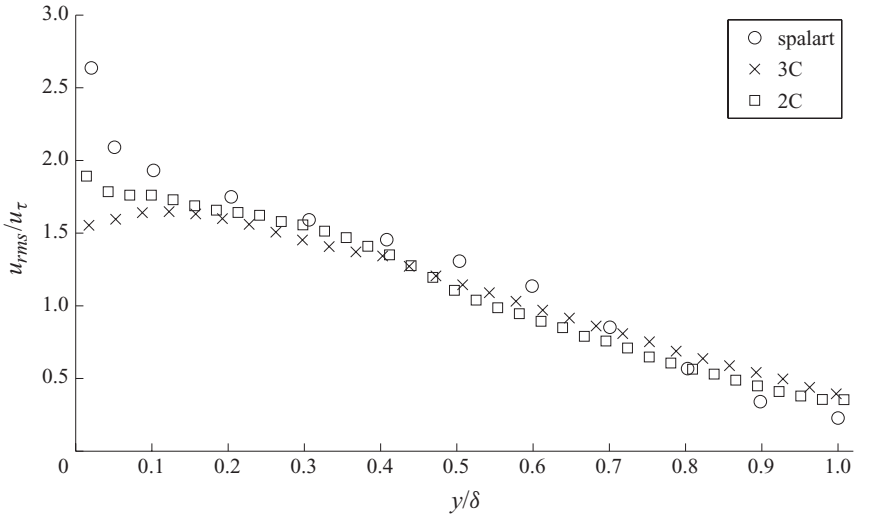


FIGURE 4. Root-mean-square streamwise velocity profile comparison.

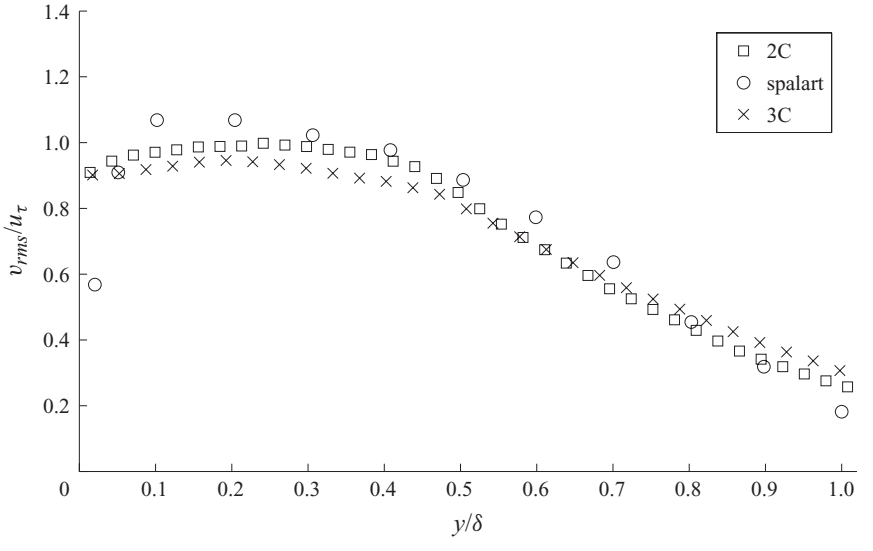


FIGURE 5. Root-mean-square wall-normal velocity profile comparison.

pertinent. As the interest of this project is on the large-scale motions, this is not viewed as a major problem.

It is also noticeable that near the edge of the boundary layer, the r.m.s. velocity is slightly overestimated. This is almost certainly due to the background noise adding to the r.m.s. velocity compared with the DNS results of Spalart (1988). This is only significant near the edge of the boundary layer because the true r.m.s. velocity in that region is so small. This is not the region of primary interest in this investigation.

Figures 5 and 6 show the wall-normal and spanwise r.m.s. velocities, respectively. It should be noted that it is not possible to plot spanwise r.m.s. for the 2C case as the spanwise component of velocity was not measured since the light sheet was oriented in the streamwise/wall-normal plane.

https://doi.org/10.1017/S0022112010006336 Published online by Cambridge University Press

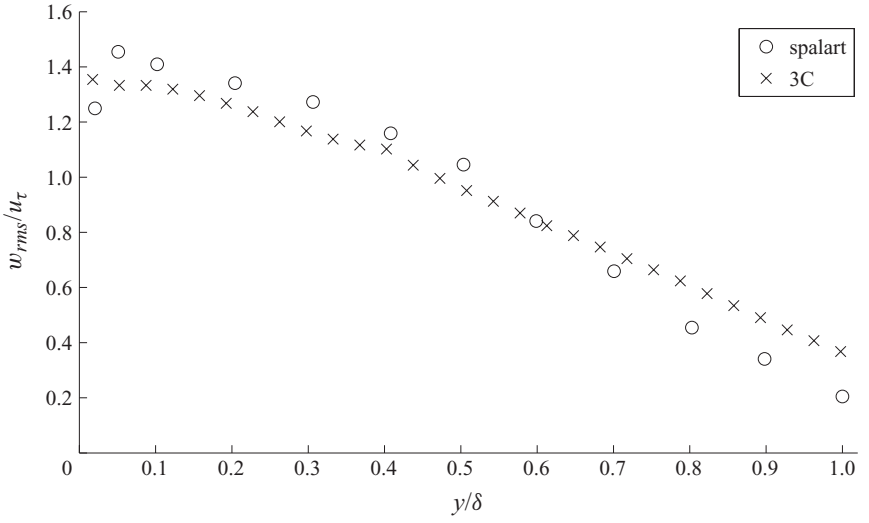


FIGURE 6. Root-mean-square spanwise velocity profile comparison.

The v_{rms} and w_{rms} velocities are seen to be a reasonable match for the expected results, with the same comments that were made for the u_{rms} velocity valid for these cases as well.

2.4. *Experimental accuracy*

When examining the flow statistics presented in § 2.3, two sources of inaccuracy are apparent. Firstly, it is clear that the spatial resolution is not sufficient to resolve the small scales of the flow. The resolution of the 3C experiment is $l = 3$ mm, which in wall units is $l^+ = l/(\nu/U_\tau) = 82$. This corresponds to around 15 Kolmogorov lengths ($\eta \approx 0.2$ mm) when Kolomogorov length is estimated by means of (2.1), where y is the value corresponding to $y/\delta = 0.4$ (approximately the prime area of interest in this investigation)

$$\eta = \left(\frac{\nu^3 \kappa y}{U_\tau^3}\right)^{1/4}. \tag{2.1}$$

This is quite large; however, the aim of this investigation is to look at large-scale flow features so it is not seen as critical. In fact, the smallest flow features that have been commented on (and have affected the conclusions) in this work have dimensions around $l^+ \approx 500$, and as such the main points are unaffected by the modest resolution used. Furthermore, the recent work by Hutchins *et al.* (2009), where the difference in turbulent stresses measured by a hot wire of length $l^+ = 79$ and a hot wire of length $l^+ = 22$ was shown to be negligible in a wall-bounded flow beyond around $y^+ = 200$, (which corresponds to around $y/\delta \approx 0.1$ in our boundary layer), indicates that the resolution of the 3C experiment in this project is adequate, as we are not investigating near-wall structures. Note that the resolution here is similar to that of the experiments reported in Hutchins & Marusic (2007*a*) in terms of their wire lengths, although for the hot-wire rake measurements they took to examine long structures (as shown in figure 1), the spacing between the probes in the rake was much larger (of the order of $1000\nu/U_\tau$). Note also that this compares well with the resolution of Elsinga *et al.* (2010)

https://doi.org/10.1017/S0022112010006336 Published online by Cambridge University Press

Due to the modest spatial resolution of the 3C results, it is possible to consider them as a low-pass filtered estimate of the true turbulent velocity field. As the focus is on the large scales, this is not a problem. Indeed, the majority of the results of this investigation are akin to flow visualisation, where the main conclusions are drawn from the flow topology: as such finely resolved results are not required.

The other source of inaccuracy is the experimental error of the PIV measurements. The turbulence intensities do not go to 0.7 % in the free stream (in which we have several wall-normal measurement locations), and as such there is some background noise in the results. The turbulence intensities in the free stream, as measured using stereoscopic-PIV are $u_{\infty,rms} = 0.016U_\infty$, (i.e. 1.6 % of the free stream velocity), $v_{\infty,rms} = 0.012U_\infty$ and $w_{\infty,rms} = 0.015U_\infty$. Since the turbulence intensities in the free stream should be approximately 0.7 % (as measured by LDA), this gives us some estimate of the error. That the u-component has the largest experimental error is not surprising, as it is the component that is perpendicular to the light sheet (i.e. goes through the thin sheet) and as such is known to be the least accurate component. The v-component involves the smallest experimental error, which is also understandable as this component can be measured independently by both cameras, and is therefore measured with greater confidence than the other two components.

Despite these limitations on the accuracy and spatial resolution of the measurements, they are more than adequate for the examination of the large-scale structures which is the focus of this paper.

2.5. *Three dimensional fields from planar PIV fields using Taylor's hypothesis*

Although the 3C results obtained directly from the experiment described in § 2.2 are interesting, they do have one shortfall, which is that they only provide the vector field in a single plane. So, although it is interesting to see all three components of the velocity vector in a plane, more insight into the turbulent boundary layer would be given by 3C velocity vectors in full 3D space, especially with regard to long structures. This is currently very difficult using any standard technique if we require a measurement volume that would be long enough to capture a significant portion of the long structures in the boundary layer with good spatial resolution. However, we can achieve full 3D results if we utilise Taylor's hypothesis to convert temporal measurements into a pseudo-spatial streamwise dimension.

The use of Taylor's hypothesis in constructing long structures in a turbulent boundary layer was discussed in detail by Dennis & Nickels (2008). That experiment (also conducted in the CUED water tunnel) enabled direct qualitative and quantitative comparisons to be made between a field constructed using Taylor's approximation and a true spatial field, up to a projection distance of 6δ. It demonstrated that Taylor's hypothesis was valid for moderate streamwise projection distances, but showed that caution must be used when projecting over long streamwise distances. It also indicated that if the interest is only in the large-scale flow features, then greater projection distances are acceptable.

It is necessary to have sufficient temporal resolution to produce a spatial resolution in the x-direction similar to that of the spatial resolution in the y- and z-directions. The use of a high-speed PIV system (described in § 2.1) easily meets that requirement. Therefore, we are able to project our time-resolved planar results into the streamwise direction over a reasonable distance, determined by careful consideration of the limitations of Taylor's hypothesis. Doing this gives us a full 3C velocity field in psuedo-3D space.

https://doi.org/10.1017/S0022112010006336 Published online by Cambridge University Press

3. Results and discussion

3.1. *Visualisation of long structures*

The low-speed regions can be visualised in 3D by using an iso-surface of the streamwise velocity fluctuation. Obviously, we need to pick an iso-value (u_{iso}) for the iso-surface, and we require that value to be negative. The iso-value chosen was 90 % of the local mean velocity ($0.9\overline{U}$), which is defined in terms of the u-fluctuation in (3.1)

$$u_{iso} = -0.1\overline{U}. \tag{3.1}$$

The iso-surface is a surface corresponding to a single value, but when we choose a low-speed value we can be confident that it encloses a region of flow that is of equal or slower speed. The converse would be true of a high-speed criterion. The choice of $u_{iso} = -0.1\overline{U}$ is therefore made as a compromise between a surface enclosing as much of the low-speed region as possible, whilst not enveloping any flow around the mean velocity, which shouldn't be included in the low-speed structure. Using $u_{iso} = -0.1\overline{U}$ is actually somewhat conservative, but it is chosen to get a clear picture of structures. It is worth noting that in figure 1 the lightest grey scale that is readily discernible corresponds to approximately $u_{iso} = -0.05\overline{U}$ and the darkest to $u_{iso} = -0.16\overline{U}$ – hence the choice here is not unreasonable. It should also be noted here that applying significant smoothing to the data would make the iso-surfaces less sensitive to the choice of levels but here we have avoided significant smoothing. This is most likely why in the data of Hutchins & Marusic (2007*a*) a level of zero is acceptable since the coarse spatial resolution in the spanwise direction (l^+ 1000) effectively smoothens their dataset. In the 3D iso-surface plots, attempting to show such a range of levels as in figure 1 would only serve to make the plots incomprehensible. The method used to investigate high-speed structures is very similar to those that are used to investigate low-speed structures. In summary, the visualisation is made using an iso-surface enclosing regions of streamwise velocity of 110 % of the mean and above, i.e. where $u_{iso} = 0.1\overline{U}$. This is the same value as used in Elsinga *et al.* (2007) and is within the range of values used by Elsinga *et al.* (2010).

Figure 7 shows four different iso-surface threshold-level choices. The percentages shown correspond to levels such that a region with a velocity less than the percentage of the free stream velocity is enclosed within the iso-surface. It is obvious from this figure (and not too surprising) that increasing the level makes it increasingly difficult to identify structures. Part of the difficulty is due to the 3D nature of these plots. If, for example, we were to choose a level of 100 %, then we would have a convoluted surface dividing the whole flow into low- and high-speed regions which would be difficult to interpret. In the bottom image, the whole flow region appears to have merged into a single structure. Consider starting from a point (a small volume) in which the velocity is lower than the mean. The probability in three dimensions of encountering a connected region that is of low speed is much higher than in two dimensions. Coupled with this is the difficulty of viewing the 3D object – background objects naturally appear connected to those in the foreground.

Adding to this is the inherent noise in PIV measurements, and hence the choice of a 100 % threshold would be meaningless. It is as well, though, to keep this sensitivity in mind when interpreting the results. Increasing the level obviously leads to the joining of structures. Note that this question of the choice of threshold on the size of structures is an issue for all previous research also, although in two dimensions the sensitivity to that choice may be less. The estimates of lengths of structures given in this paper are for the contour level chosen and will depend on the choice of this level.

https://doi.org/10.1017/S0022112010006336 Published online by Cambridge University Press

https://doi.org/10.1017/S0022112010006336 Published online by Cambridge University Press

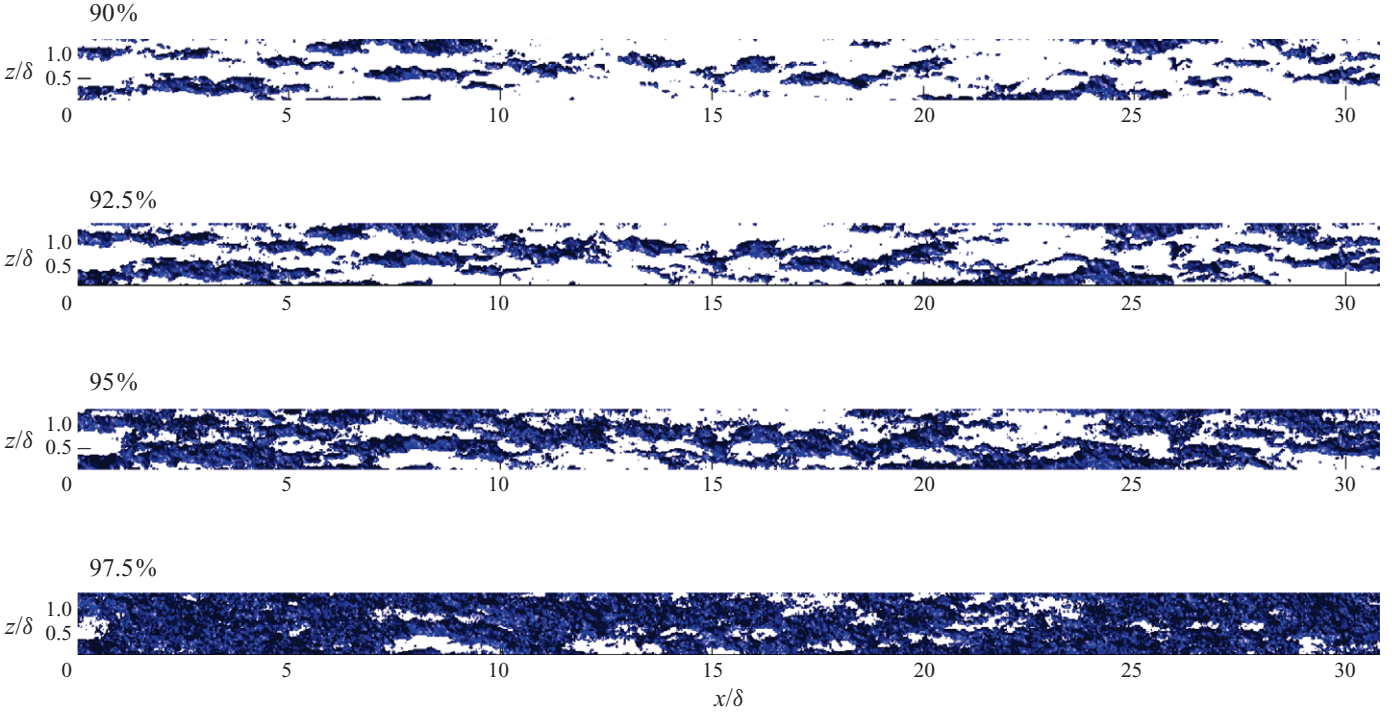


FIGURE 7. (Colour online) The effect of using different iso-surface levels of streamwise fluctuation for visualising structures.

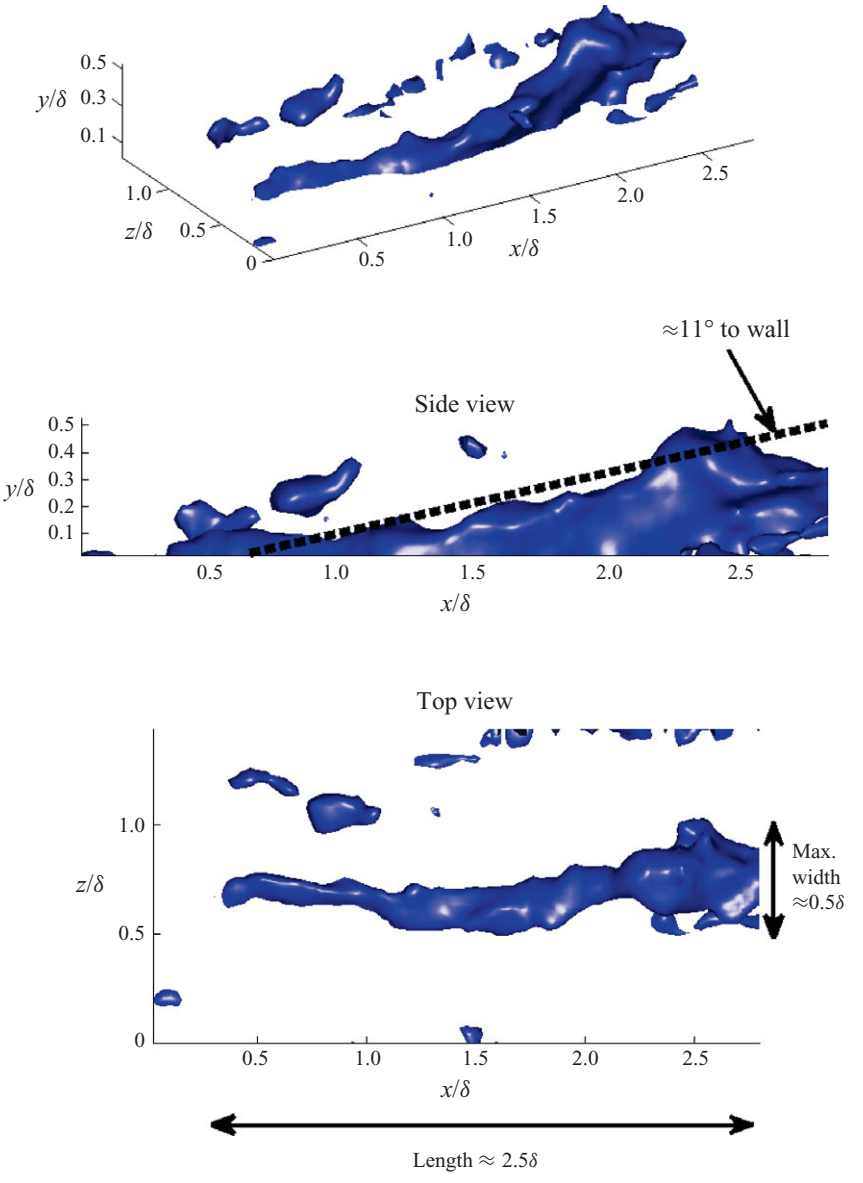


FIGURE 8. (Colour online) Example of the characteristics of a relatively short low-speed structure.

Nevertheless, many of the qualitative results – in particular relating to the shapes of the structures are much less sensitive to this choice.

In summary then when considering such long low- (or high-) speed regions in turbulent boundary layers, great care must be taken. Two significant points are that smoothing (either direct or due to spatial resolution effects) will tend to join structures and give the impression of longer features. Choosing a higher iso-level (i.e. further from the mean) may have the opposite effect of reducing the length of these structures.

An example of an iso-surface is plotted in figure 8; it shows a distinct region of low momentum elongated in the streamwise direction, as observed by previous researchers

https://doi.org/10.1017/S0022112010006336 Published online by Cambridge University Press

such as Hutchins & Marusic (2007*a*). It is at least five times as long as it is wide (using its maximum width). It extends down to the wall for the vast majority of its length, whilst its upper surface is at an angle of approximately 11° to the wall; hence, the height of the structure is increasing slowly with downstream distance, reaching a maximum of 0.5δ, which is similar to its width. The surface of the structure is clearly uneven and wavy in all directions, although in this example we do not see any large meandering. This is perhaps not so surprising as this particular structure is not as long as the superstructures, which we would expect to meander.

A longer low-speed structure (actually the longest structure found in this dataset) is shown in figures 9 and 10. The total length of this structure is 8.4δ. Despite the increase in length in comparison to the structure in figure 8, the maximum width is quite similar ($\approx 0.5\delta$) and the maximum height is only slightly larger, with the structure now reaching a height of $y/\delta \approx 0.6$. From examining the side view in figure 10, it is clear that we cannot choose an angle to the wall which characterises the entire 8.4δ length of the structure. However, as shown in figure 10, it is possible to see two separate regions of the structure where the angle to the wall of the upper surface is around 10°. Therefore, this long structure seems to consist of two ramps of streamwise length $\approx 3\delta$ with a characteristic angle of 10°. Or, to view it another way, the structure in figure 9 is made up of two structures similar to that in figure 8 aligned end-to-end. The longer, combined, structure is seen to meander much more than the shorter structure. The top view in figure 10 shows a significant meandering at around $x/\delta = 5$ in particular. Bearing in mind the above discussion of whether we regard the longer structure as an entity by itself or as an agglomeration of two shorter structures, we could interpret this change of direction as a joining point of two slightly misaligned shorter structures or as just a region where one long structure is meandering.

3.2. *The length of long structures*

The examination of individual realisations of low-speed structures has shown that they are elongated in the streamwise direction. However, there is clearly some variation in the streamwise length of these structures, the two examples shown above being 2.5δ and 8.4δ, respectively. The correlation of u (Dennis & Nickels 2011) also shows a significant elongation in the streamwise direction, with a significant correlation extending to $\approx 5\delta$. We will now examine the length distribution of long structures in this flow.

A histogram of low-speed structures binned according to their streamwise length is shown in figure 11. The length is found by locating the start of a structure (the most upstream location of the iso-surface) and then searching downstream within the iso-surface until the most downstream point within the surface is found. Only structures of length greater than 2δ have been included in the histogram, as we are only going to consider structures of significant streamwise elongation. It should be noted that there are many structures that show up to be less than 2δ in streamwise length but are not seen as significant whilst we are particularly considering long structures. It should be emphasised here that the precise lengths found will depend on the iso-surface level defined to characterise the structures. The main interest here is in the approximate distribution of lengths rather than their precise values, and changing the level within a reasonable margin does not alter the distribution greatly.

Figure 11 demonstrates that in general, structures are not found to be very long. Almost half of those included in this analysis are 2–3δ in length. These would correspond with the 'large-scale motions' (LSMs) observed by Balakumar & Adrian (2007). In boundary-layer flows, they denoted structures of lengths ranging from

https://doi.org/10.1017/S0022112010006336 Published online by Cambridge University Press

https://doi.org/10.1017/S0022112010006336 Published online by Cambridge University Press

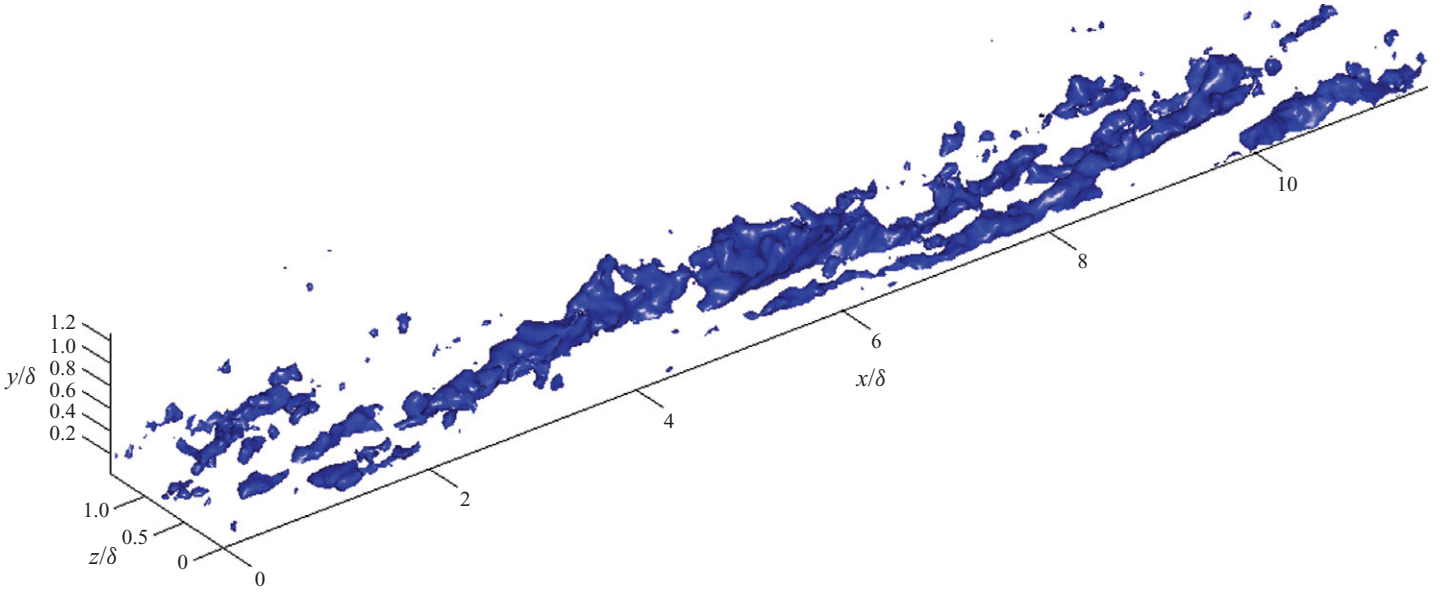


FIGURE 9. (Colour online) Example of a long low-speed structure.

https://doi.org/10.1017/S0022112010006336 Published online by Cambridge University Press

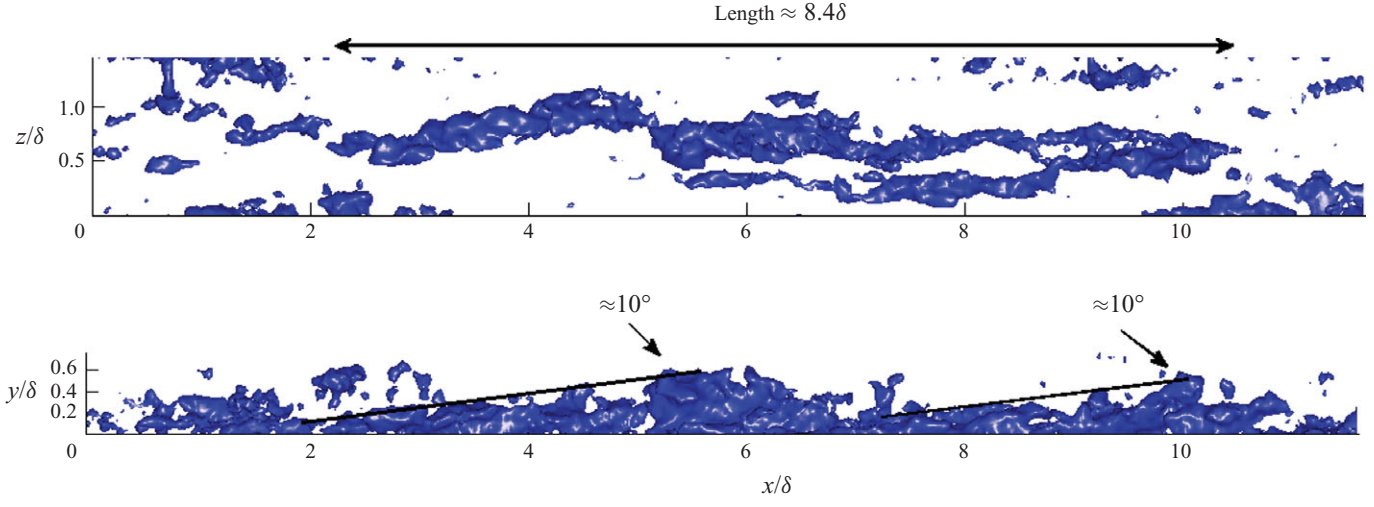


FIGURE 10. (Colour online) Example of the characteristics of the long low-speed structure shown in figure 9 (top and side view).

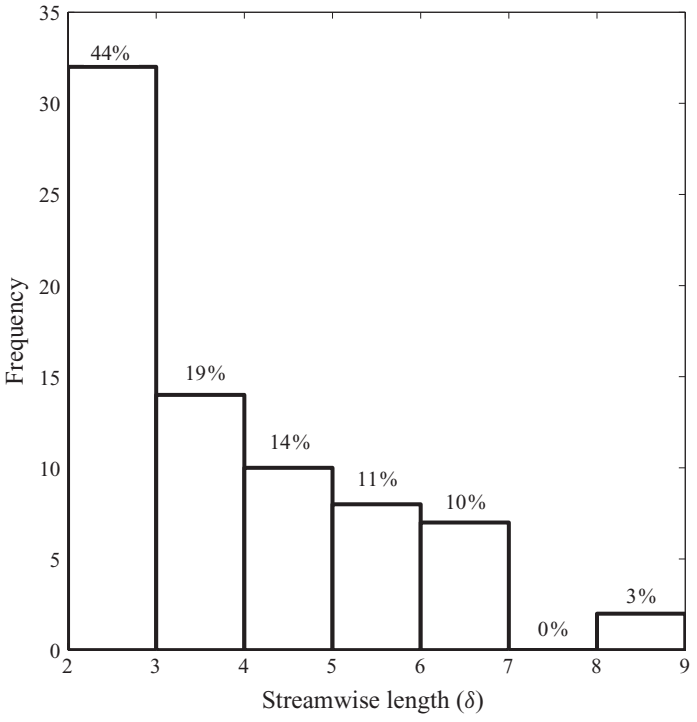


FIGURE 11. Histogram of the streamwise length of low-speed regions for a sample size of 73. Only regions of length $>2\delta$ are considered. Note that percentages add up to 101 due to rounding.

approximately 1δ to 3δ as LSMs and structures greater than 3δ as very large-scale motions (VLSMs). According to this (somewhat arbitrary) division then, 44 % of the structures would be LSMs and the remainder VLSMs. Nearly all (97 %) are found to be below 7δ in total length. This is interesting in the light of some of the previous results from the literature, such as in Hutchins & Marusic (2007*a*) and Ringuette *et al.* (2008), where long structures were found to be of much greater length ($>20\delta$); these motions would be classified as VLSMs by Balakumar & Adrian (2007). The significant difference between those results that found structures of such long lengths and the current result is that those lengths were reached by visual inspection of 2D fields. With our 3D field, it is not possible to visualise the results without choosing some kind of criteria. In our case, we have used an iso-surface of streamwise velocity fluctuation. This criterion, and the lengths measured using it (simply measured by taking the difference between the beginning and end of each iso-surface in the x-direction), are more objective than the visual inspection method. The eye will tend to smooth over small areas that perhaps do not fit in with the large feature of the flow, and as mentioned earlier, large measurement areas often correspond with limited spatial resolution, which would act to smooth and join shorter structures into longer structures.

A histogram of the high-speed structures binned by streamwise length is shown in figure 12. This can be compared to its low-speed counterpart in figure 11. The two histograms are very similar in their general distribution, and therefore most of the discussion regarding low-speed structures can also be applied to high-speed structures. The main difference is that high-speed structures are somewhat more

https://doi.org/10.1017/S0022112010006336 Published online by Cambridge University Press

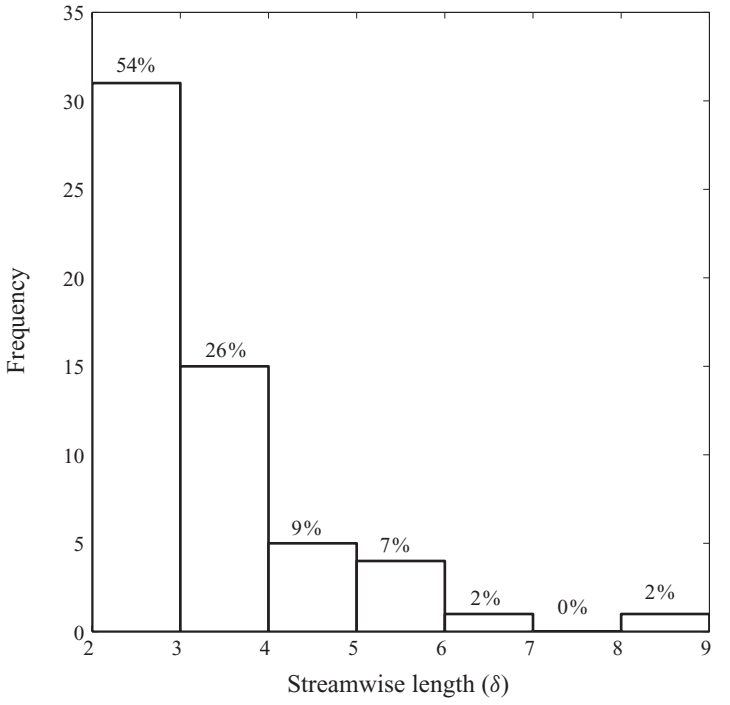


FIGURE 12. Histogram of the streamwise length of high-speed regions.

weighted towards the shorter end of the distribution between 2 and 4δ. Overall, we can conclude that the length distribution of high- and low-speed structures is generally similar, with long low-speed structures found to be slightly longer.

One way to interpret these results is to assume that superstructures ($>20\delta$) are the result of several long structures ($<7\delta$) aligning in the streamwise direction. This has been suggested and discussed before (e.g. Kim & Adrian 1999). This alignment may have led previous researchers to visually join long structures into superstructures. A good piece of evidence to support this theory is the correlation of the streamwise velocity fluctuation shown in Dennis & Nickels (2011). The correlation shown in that figure is of the order of 5δ, and is strong only over approximately 2δ. This corresponds much better to the histogram of figure 11, which shows generally that long structures are shorter than 7δ and are mostly between 2δ and 3δ in length, than it does to the 20δ long superstructures, albeit that we could also explain the difference by the meandering nature of superstructures (see Hutchins & Marusic 2007*a*). The fact that the long structures align to make superstructures is obviously interesting in itself. To confirm the existence of this alignment, we can examine the 3D fields over very long domains.

Viewing iso-surface plots over long domains makes picking out individual structures very difficult, as the domain appears to be overcrowded with surfaces. To get around this problem, we have calculated points along the 'spine' of the low-speed structures by taking the centre of the region the iso-surface encloses at many x locations along its length. Plotting all these points enables visualisation of the position and length of the long structure, as well as (up to a point) its meandering. We lose height and width information by doing this but they are not as important for this exercise, and the benefit of clarity is the reward. These spines have been plotted for 10 different

https://doi.org/10.1017/S0022112010006336 Published online by Cambridge University Press

https://doi.org/10.1017/S0022112010006336 Published online by Cambridge University Press

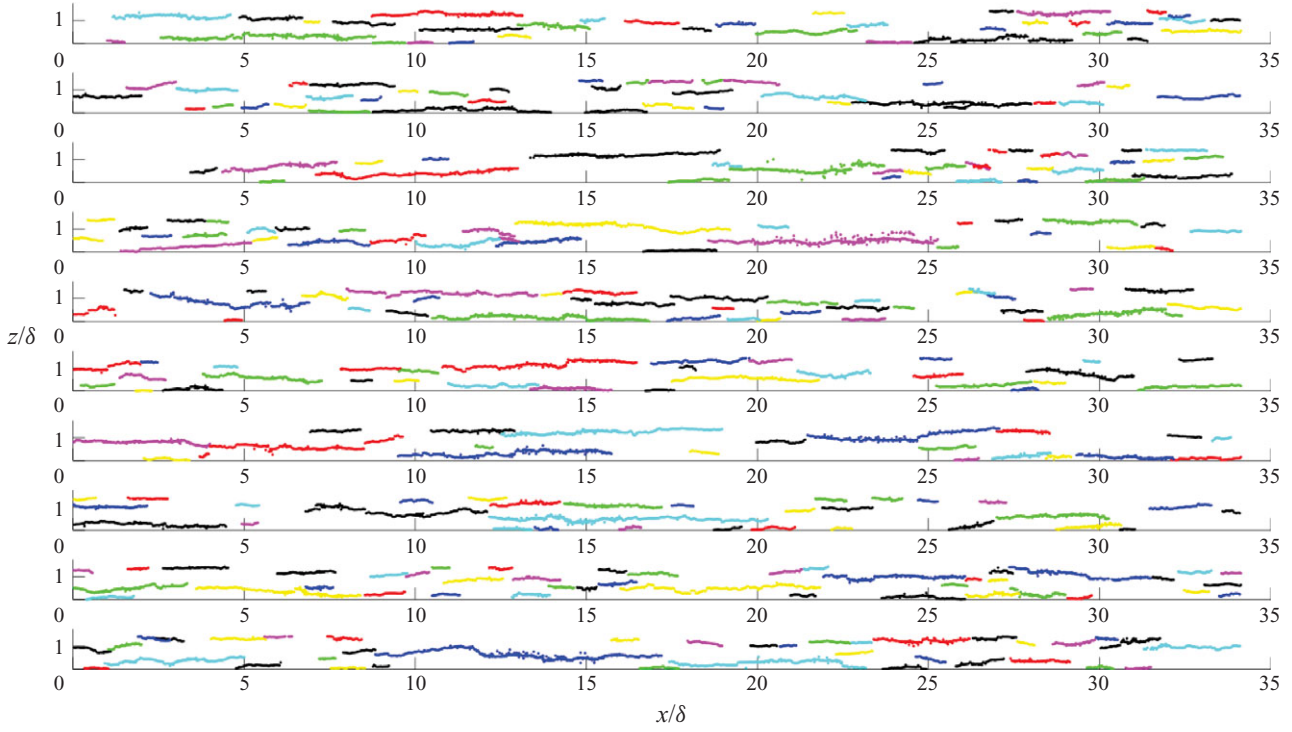


FIGURE 13. (Colour online) Alignment of spines of low-speed long structures over a long domain.

runs in figure 13. Each individual low-speed structure is plotted in a different colour; however, as the reader will notice, colours are repeated due to the lack of sensible colours to plot in, although this should not cause too much confusion as spines of the same colour that are large distances apart have obviously not been classed as a single structure.

What figure 13 shows quite clearly is that many of the structures do indeed align with each other. This supports the theory that the individual structures we have found to be $2 < x/\delta < 7$ align to form superstructures of much greater lengths. We can certainly pick out structures that have aligned to create superstructures of 10δ and over from figure 13. It should be pointed out that there are various reasons why these structures have been kept separate using the iso-surface method. Two are obvious from figure 13: sometimes there is a small streamwise gap between the structures, and sometimes the structures are slightly misaligned in the spanwise direction whilst the start of one is close to the end of another in the streamwise direction. Smoothing the results either due to spatial resolution (e.g. Hutchins & Marusic 2007*a*) or deliberately (Ringuette *et al.* 2008) would tend to join these structures and hence lead to much longer features. There is a third reason that cannot be appreciated from figure 13, which is that the ends of two seemingly adjoining structures are at different wall-normal locations, and hence cannot be joined by the same surface.

It is not known whether the alignment of the long structures into very long structures occurs simply by chance or whether there is a mechanism leading to the alignment. Chance alignment is certainly a possibility that cannot (at this stage) be discounted. An alignment by chance would lead to a similar distribution of lengths, with very long structures occurring less frequently than shorter structures.

3.3. *The frequency of long structures*

The grand total of long structures in the dataset under consideration here is 333 low-speed structures and 289 high-speed structures. A structure here is classed as any region enclosed by the u_{iso} iso-value that is greater than 0.5δ in length in the streamwise direction. This condition was enforced simply to remove the many small blobs that otherwise occurred, which, although they are probably not all noise, are not important when considering coherent structures, as the structure needs to present coherence over a region of significant size.

To put the regularity of these structures into more useful terms, the dataset spread over 340δ in the x-direction, 1.75δ in the z-direction and the full height of the boundary layer; hence, low-speed structures occur once every 1.02δ, whilst high-speed structures occur once every 1.18δ. As the length of many of these structures is greater than 1δ, this means we actually have more than a 98 % chance of having a low-speed structure and 82 % chance of having a high-speed structure, in a domain of length δ. In fact, if all the structures found in the 340δ were laid end-to-end, they would stretch for 439δ in the low-speed case and 410δ in the high-speed case. Normalising these numbers by the domain length, we have, on average, low-speed structures 129 % the length of the domain and high-speed structures 121 % the length of the domain. This implies that we would expect to find one or more structures of both the low- and high-speed varieties at any given x-location in the boundary layer, for a domain of width $z/\delta = 1.75$. In short, both low- and high-speed structures are found to be common in boundary-layer flow.

From these numbers, it is apparent that the regularity of low- and high-speed structures is similar. They do not appear in a 1 : 1 ratio as they would if they were *always* found as a pair, but a 1.15 : 1 ratio in favour of low-speed structures (based

https://doi.org/10.1017/S0022112010006336 Published online by Cambridge University Press

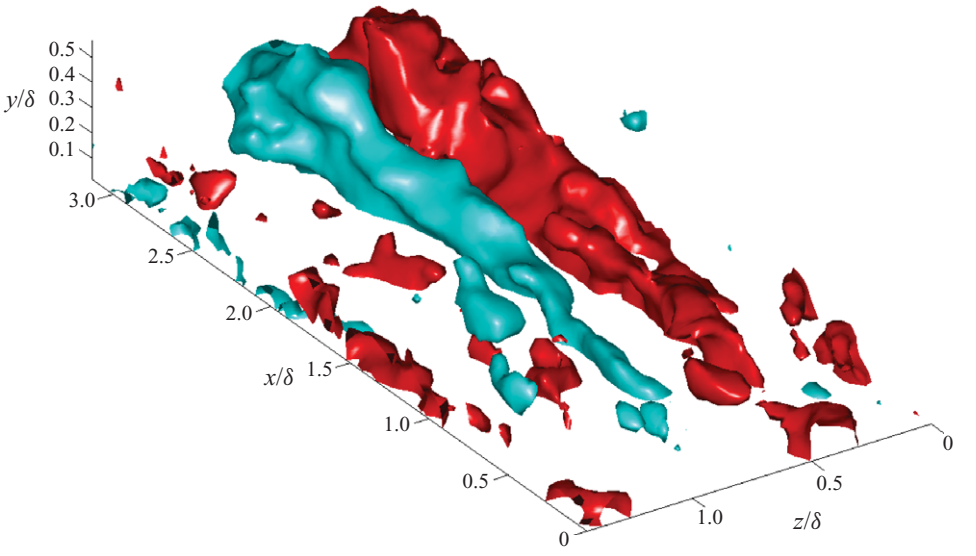


FIGURE 14. (Colour online) 3D iso-surface representation of high- and low-speed long structures side-by-side. Blue: $u_{iso} = -0.1\overline{U}$ (low speed), red: $u_{iso} = 0.1\overline{U}$ (high speed).

on quantity). In terms of total cumulative length of structures, the ratio is just 1.07 : 1 in favour of the low-speed structures.

3.4. *The relationship between high- and low-speed long structures*

It has been noted from 2D results of previous researchers that it is quite common for high- and low-speed long structures to be found side-by-side, an arrangement that also fits with the presence of a vortical motion. However, in § 3.3, we also established that overall, high- and low-speed long structures do not appear as pairs of the same length. Therefore, the probability of high- and low-speed long structures being found together is of interest.

Figure 14 shows one example where the high- and low-speed long structures do appear as a pair. It is actually the low-speed long structure shown in figure 8, with the addition of the positive iso-surface shown in red. This figure shows high- and low-speed long structures side-by-side having very similar lengths, widths and angles to the wall. Although this instantaneous picture shows that such a pair of structures is possible, it is not found to be common in the turbulent boundary layer in general.

This is illustrated by figure 15, which shows a 'spine' plot similar to that of figure 13. In fact, it is the low-speed long structures from figure 13 shown in blue, in addition to the high-speed long structures plotted in the same way (and shown in red). From this plot, we can make a better judgement about the relationship between high- and low-speed long structures in general. The following are apparent.

(i) Generally, when proceeding in the z-direction, high- and low-speed long structures are found to alternate. The high- and low-speed long structures do appear side-by-side to some extent, and it is very rare to have two structures of the same type (i.e. two high-speed or two low-speed) side-by-side.

(ii) Although we often find high- and low-speed structures side-by-side, they are rarely 'pairs' in the sense that they have different lengths, and do not identically share the other characteristics displayed by the pair in figure 14.

https://doi.org/10.1017/S0022112010006336 Published online by Cambridge University Press

https://doi.org/10.1017/S0022112010006336 Published online by Cambridge University Press

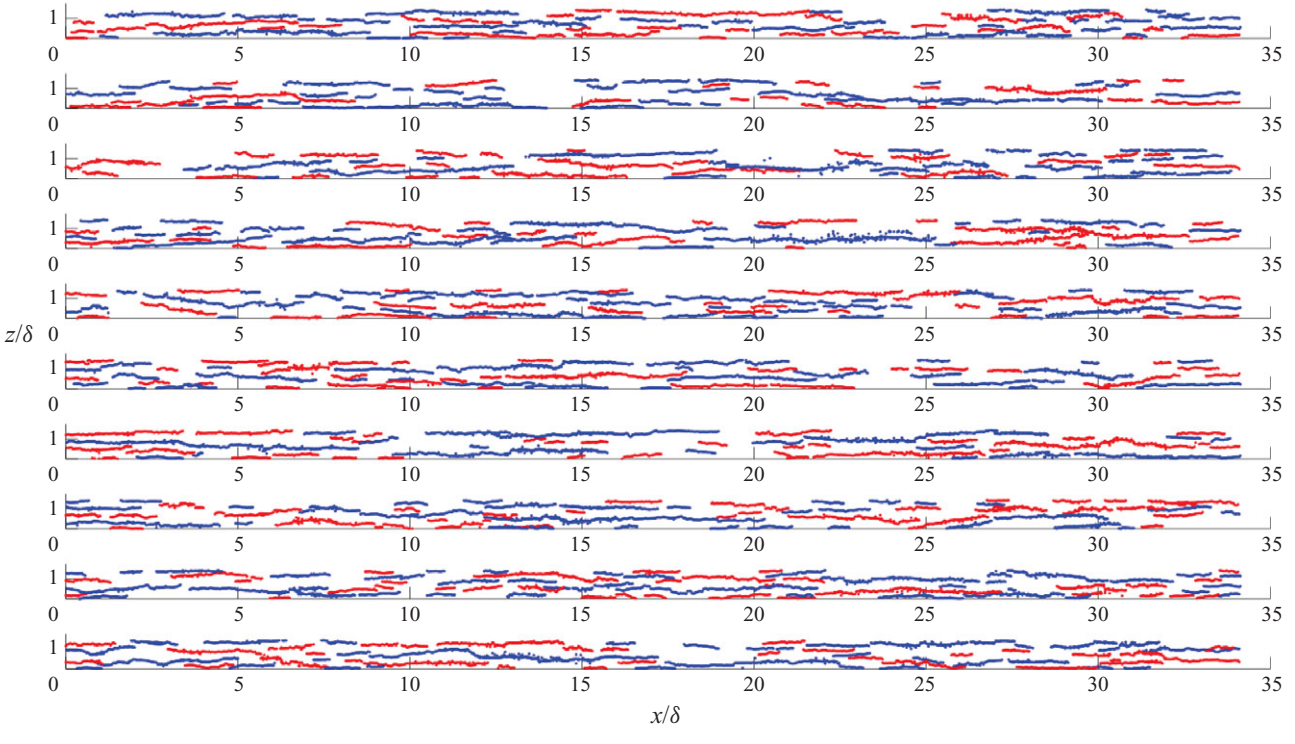


FIGURE 15. (Colour online) Spines of low (blue) and high (red) speed structures over a long domain.

It seems reasonable to assert that there is a relationship between high- and low-speed long structures. They obviously have similarities in average size, and their locations appear to be dependent on each other. In general, the high-speed structures are slightly shorter. It therefore seems unlikely that high- and low-speed structures are related in an 'equal and opposite' sense, and this is reinforced by the lack of clear pairing of their locations. Instead, it seems that perhaps they are related because they are formed by the same mechanism, but this mechanism favours low-speed structures, and makes them more distinct, i.e. gives them stronger characteristics than high-speed structures. This could be explained by the hairpin vortex model as such a vortex (even if it is asymmetric) would produce a stronger low-speed region than a high-speed region due to the contribution from the vortex head.

3.5. *The height of long structures in the boundary layer*

It should be noted that in all the examples of high- and low-speed long structures given so far, the structures generally extend to the wall but do not extend to the edge of the boundary layer. This is found throughout the dataset, with structures generally not found much above $y/\delta = 0.5$ (by inspection).

Figure 16 shows a top-down example of the high- and low-speed structures plotted using the iso-surface method, and then slices of the same field at different heights in the boundary layer (as marked). The first slice at $y/\delta = 0.15$ shows that the high- and low-speed regions are certainly present at this height in the boundary layer. Their streamwise elongation is clear and, in fact, this single slice is quite a good representation of what is present in the 3D field, as it is clear that this slice maps well onto the top-down view of the 3D structures shown. (This also goes some way toward showing that the structures we are finding with the $u_{iso} = \pm 0.1\overline{U}$ iso-surfaces are the same ones, and are of a similar length, to the structures that are clear to the eye in the 2D wall-parallel slices.)

Moving higher in the boundary layer, to $y/\delta = 0.32$, the slice shows that regions of strong positive and negative fluctuations are present; however, it does not show a great deal of streamwise elongation. This implies that whilst the long structures do have a presence in this region of the boundary layer, the whole of their length is not felt at this height. This makes sense when we consider the characteristic angle that long structures have to the wall, which, although it is only shallow, means that the upper end of the structure is at a significantly higher level than the lower end due to the long length of the structure.

By $y/\delta = 0.49$, there are very few regions of strong fluctuations and there is very little in the way of streamwise elongation. At this level, we are only getting the tips of the very highest structures. Above this level, at $y/\delta = 0.65$ and $y/\delta = 0.82$, we only see blobs of very weak fluctuations that have no streamwise elongation at all. Large areas of these slices are seen to be at approximately the mean flow speed (green colour), especially $y/\delta = 0.82$. It is clear from these slices that high- and low-speed structures are only elongated in the lower half of the boundary layer, and to appreciate the length of the structures fully we need to be looking below $y/\delta = 0.3$, as at this kind of height we are only seeing the presence of the upper ends of the long structures.

We can of course check that this observation is correct using our database of long structures. Figure 17 shows a histogram of the maximum height (h) that structures reach in the boundary layer. It includes both high- and low-speed structures from a sample of 622. Figure 17 does indeed show a strong tendency for structures to stay below $y/\delta = 0.5$. To be precise, 80 % of the structures in this sample were found to

https://doi.org/10.1017/S0022112010006336 Published online by Cambridge University Press

https://doi.org/10.1017/S0022112010006336 Published online by Cambridge University Press

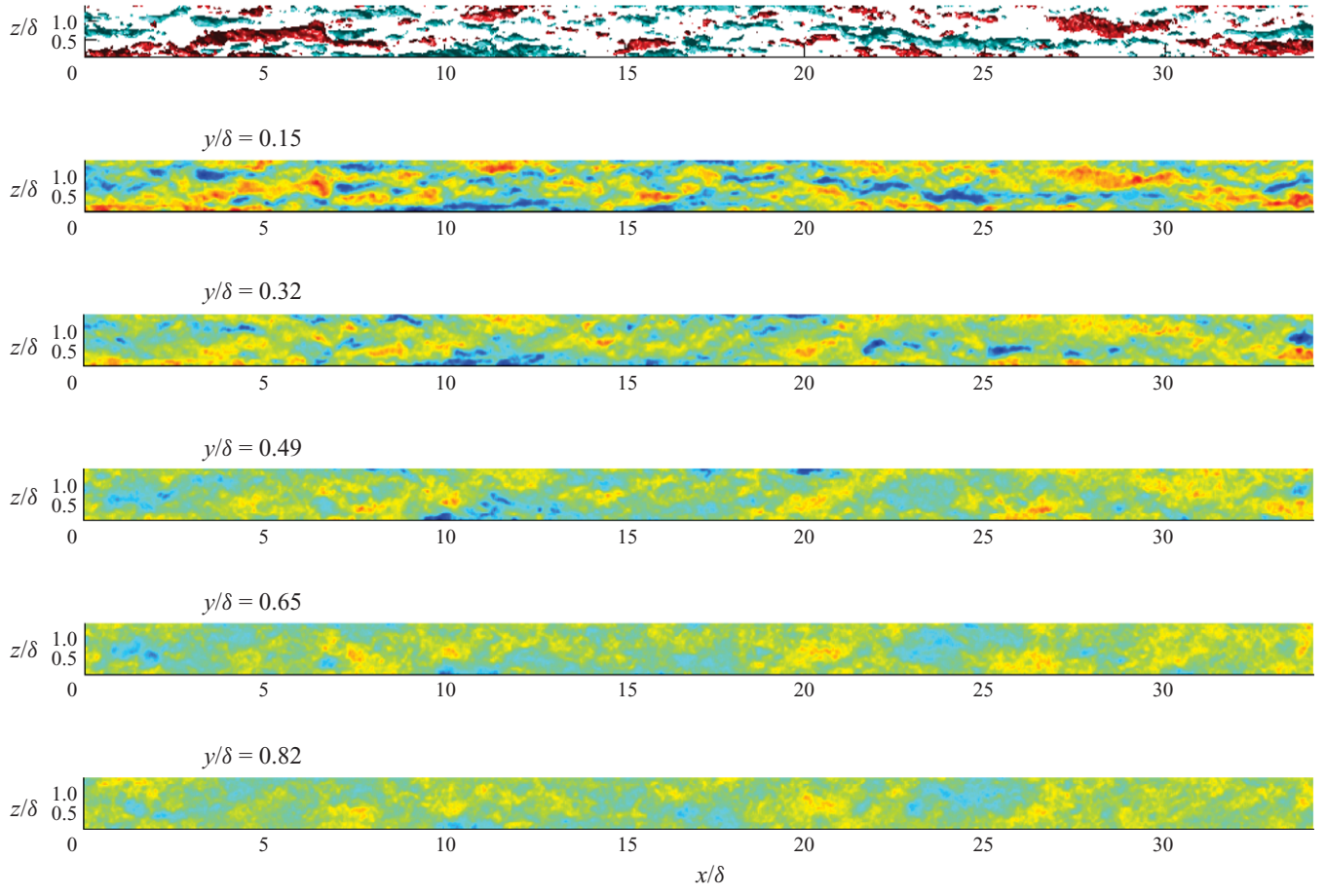


FIGURE 16. (Colour online) Top view of high- and low-speed structures and slices at different heights in the boundary layer.

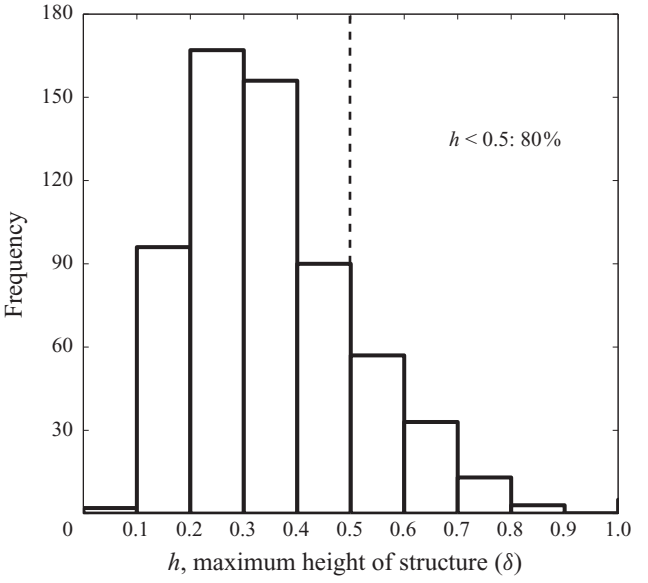


FIGURE 17. Histogram showing the number of long structures binned according to the maximum height (h) they reach in the boundary layer.

stay below $y/\delta = 0.5$. So, there are some structures that do extend higher into the boundary layer, but these are rare, especially above $y/\delta = 0.6$.

3.6. *The wall-normal velocity fluctuation*

The wall-normal velocity fluctuation (v) can be visualised in 3D in a similar way to u fluctuation by using iso-surfaces. Instead of using some factor of the local mean velocity, it is more sensible to use some factor of the local v_{rms}. We have chosen a value of $v_{iso} = \pm 1.3 v_{rms}$, which gives us a visualisation of those regions in which there is a fluctuation significantly stronger than the average. This is a somewhat arbitrary parameter; indeed it is actually chosen to give a clear result rather than for any physical reason. However, as we are simply using it for visualisation purposes, the exact numbers involved here are actually only of minimal interest.

A double plot of a top-down view of iso-surfaces of strong streamwise and wall-normal fluctuations is shown in figure 18. The blue and cyan plot shows low-speed structures (blue), together with regions of strong upward movement in the wall-normal direction, i.e. large $v > 0$ (cyan). The red and magenta plot shows high-speed structures (red), together with regions of strong downward movement in the wall-normal direction, i.e. large $v < 0$ (magenta). What is quite obvious from the two plots is that there is a clear association between $u < 0$ and $v > 0$ (blue and cyan) and $u > 0$ and $v < 0$ (red and magenta). Areas of upward movement are found in, around and above areas of low streamwise speed, and areas of downward movement are found in, around and above areas of high streamwise momentum. This pattern is observed to appear throughout the dataset similarly to the example shown.

In the context of sweeps, ejections and the commonly employed quadrant analysis, it is apparent that the blue and cyan iso-surfaces are representative of Q2 (ejection) events, and the red and magenta iso-surfaces are representative of Q4 (sweep) events. Therefore, long structures can be associated with a quadrant event depending on the sign of the streamwise fluctuation, i.e. Q2 events are associated with low-speed long

https://doi.org/10.1017/S0022112010006336 Published online by Cambridge University Press

https://doi.org/10.1017/S0022112010006336 Published online by Cambridge University Press

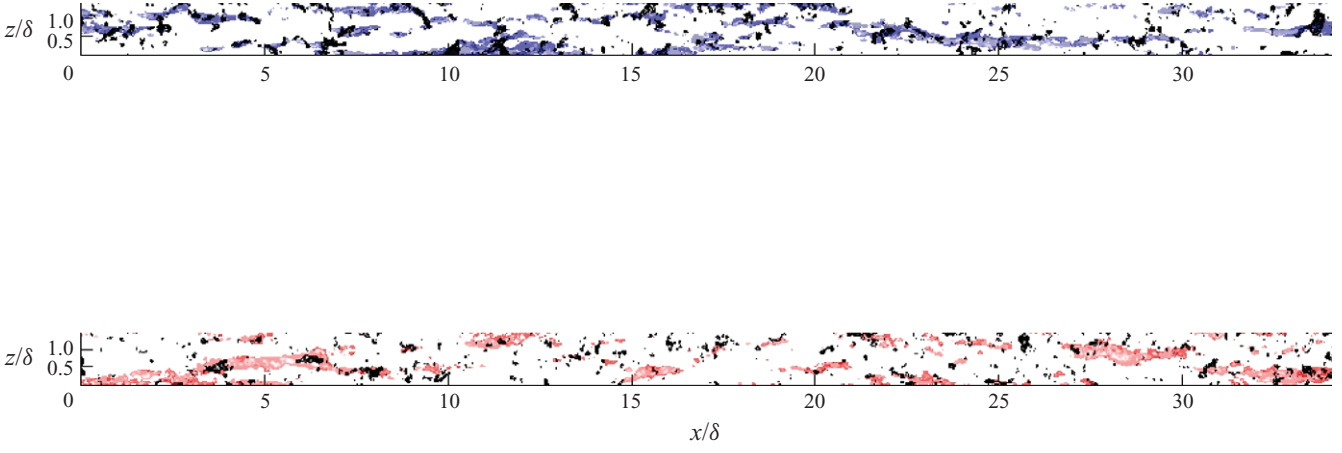


FIGURE 18. (Colour online) Iso-surfaces of streamwise and wall-normal fluctuations. (*a*) $v_{iso} = 1.3v_{rms}$ (black) on $u_{iso} = -0.1\overline{U}$ (blue). (*b*) $v_{iso} = -1.3v_{rms}$ (black) on $u_{iso} = 0.1\overline{U}$ (red).

https://doi.org/10.1017/S0022112010006336 Published online by Cambridge University Press

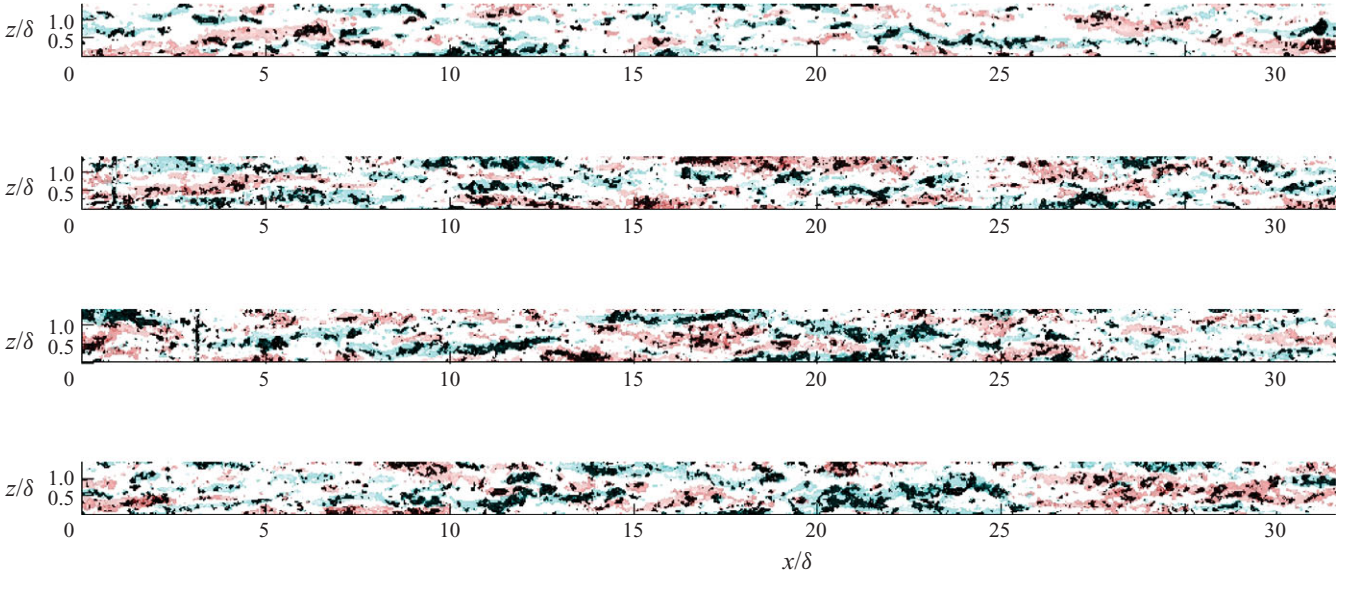


FIGURE 19. (Colour online) Black iso-surfaces of high Reynolds stress ($-uv$) against a background of high (red) and low (blue) speed structures.

structures, and Q4 events are associated with high-speed long structures. This is an interesting feature of long structures as it gives the velocity vector associated with them a characteristic angle, rather than it being a purely streamwise phenomenon. This has implications for the orientation of the flow feature (e.g. vortex) that may be associated with long structures. It is also important to note that the regions highlighted by the iso-surfaces of v are not elongated shapes, as those of u are. Instead, they are numerous small 'bubbles' that run along the elongated shape made by the u iso-surface. The size of these bubbles is obviously determined by the choice of v_{iso}; however, it is clear that the v iso-surface will never appear as an elongated volume like the u iso-surfaces do.

Another important aspect of this observation is the implication for the Reynolds shear stress. Obviously, both the low-speed/upward movement ($u<0,\ v>0$) and the high-speed/downward movement ($u>0,\ v<0$) increase the Reynolds shear stress ($-uv$). Therefore, this implies that these long structures have a strong influence on the Reynolds shear stress. We can check the relationship between long structures and the Reynolds shear stress by plotting regions of high $-uv$ on top of the high- and low-speed structures. This is shown in figure 19, where the result is a very clear relationship between long structures and the Reynolds shear stress. There are even regions where the $-uv$ iso-surface is elongated to a similar length as the long structures. This is particularly true of the Reynolds shear stress associated with low-speed structures, which is seen to be more significant than that associated with high-speed structures. This reinforces the view expressed in § 3.4 that generally high-speed structures have weaker characteristics than low-speed structures. Overall, one is compelled to think that long structures of this kind are playing an important part in the dynamics of the turbulent boundary layer.

4. Conclusions

Experiments have been conducted to produce full 3D velocity fields of a moderate Reynolds number turbulent boundary layer via the use of Taylor's hypothesis. All the results produced by this experiment showed indications that long structures are a ubiquitous feature of turbulent boundary-layer flow. The instantaneous velocity fields and a variety of flow-field statistics all demonstrated the presence of both high- and low-speed long structures that had reasonably consistent characteristics.

Iso-surface visualisations from the 3D fields show that high- and low-speed long structures of varied lengths are common. Examples showed that the angle to the wall of the iso-surfaces was around 11°, and there were indications that the very long structures were possibly made up of multiple shorter structures.

Statistics on the length of long structures showed that very long structures were rare, generally they were no longer than 7δ and most were much shorter, with high-speed long structures generally being slightly shorter than their low-speed counterparts. There were clear signs that a significant number of long structures appeared to be aligned (in the streamwise direction) with other long structures. On average, there is at least one long structure of each type present at every streamwise location in the results, demonstrating that long structures are common. The long structures were mostly found in the lower half of the boundary layer with the maximum height of 80 % of the structures being less than $y/\delta=0.5$.

Examination of the wall-normal fluctuation (v) showed an association between it and the long structures such that $u<0$ and $v>0$ were found together, and similarly, there was an association between $u>0$ and $v<0$. Thus, low-speed long structures are associated with Q2 events and high-speed long structures with Q4 events. Hence,

https://doi.org/10.1017/S0022112010006336 Published online by Cambridge University Press

long structures in general are regions of increased Reynolds shear stress. Regions of positive $-\overline{uv}$ seem to be particularly correlated with the low-speed structure, whereas the same is not true of the high-speed long structures.

Overall, the study has given new insight into the 3D nature of the long structures observed in turbulent boundary layers, their statistics and their relationship to the important turbulence quantities.

Sadly, Dr Timothy B. Nickels died on 2 October 2010, shortly after the submission of this paper.

REFERENCES

Abe, H., Kawamura, H. & Choi, H. 2004 Very large-scale structures and their effects on the wall shear-stress fluctuations in a turbulent channel flow up to $Re_\tau = 640$. *J. Fluids Engng* **126**, 835–843.

Adrian, R. J. 2007 Hairpin vortex organization in wall turbulence. *Phys. Fluids* **19** (4), 041301 (1–16).

Balakumar, B. J. & Adrian, R. J. 2007 Large- and very-large-scale motions in channel and boundary-layer flows. *Phil. Trans. R. Soc.* A **365**, 655–681.

Clauser, F. 1956 The turbulent boundary layer. *Adv. Appl. Mech.* **4**, 1–51.

Dennis, D. J. C. & Nickels, T. B. 2008 On the limitations of Taylor's hypothesis in constructing long structures in a turbulent boundary layer. *J. Fluid Mech.* **614**, 197–206.

Dennis, D. J. C. & Nickels, T. B. 2011 Experimental measurement of large-scale three-dimensional structures in a turbulent boundary layer. Part 1. Vortex packets. *J. Fluid Mech.* doi:10.1017/S0022112010006324.

Elsinga, G. E., Adrian, R. J., van Oudheusden, B. W. & Scarano, F. 2010 Three-dimensional vortex organization in a high-Reynolds-number supersonic turbulent boundary layer. *J. Fluid Mech.* **644**, 35–60.

Elsinga, G. E., Kuik, D. J., van Oudheusden, B. W. & Scarano, F. 2007 Investigation of the three-dimensional coherent structures in a turbulent boundary layer with tomographic-PIV. In *Proc. 45th AIAA Aerospace Sciences Meeting*, Reno, NV, January 8–11.

Ganapathisubramani, B., Clemens, N. T. & Dolling, D. S. 2006 Large-scale motions in a supersonic turbulent boundary layer. *J. Fluid Mech.* **556**, 271–282.

Ganapathisubramani, B., Lakshminarasimhan, K. & Clemens, N. T. 2008 Investigation of three-dimensional structure of fine scales in a turbulent jet by using cinematographic stereoscopic particle image velocimetry. *J. Fluid Mech.* **598**, 141–175.

Ganapathisubramani, B., Longmire, E. K. & Marusic, I. 2003 Characteristics of vortex packets in turbulent boundary layers. *J. Fluid Mech.* **478**, 35–46.

Guala, M., Hommema, S. E. & Adrian, R. J. 2006 Large-scale and very-large-scale motions in turbulent pipe flow. *J. Fluid Mech.* **554**, 521–542.

Hutchins, N. & Marusic, I. 2007*a* Evidence of very long meandering features in the logarithmic region of the turbulent boundary layers. *J. Fluid Mech.* **579**, 1–28.

Hutchins, N. & Marusic, I. 2007*b* Large-scale influences in near-wall turbulence. *Phil. Trans. R. Soc.* A **365**, 647–664.

Hutchins, N., Nickels, T. B., Marusic, I. & Chong, M. S. 2009 Hot-wire spatial resolution issues in wall-bounded turbulence. *J. Fluid Mech.* **635**, 103–136.

Kim, K. C. & Adrian, R. J. 1999 Very large-scale motion in the outer layer. *Phys. Fluids* A **11** (2), 417–422.

Monty, J. P., Stewart, J. A., Williams, R. C. & Chong, M. S. 2007 Large-scale features in turbulent pipe and channel flows. *J. Fluid Mech.* **589**, 147–156.

Ringuette, M. J., Wu, M. & Pino Martin, M. 2008 Coherent structures in direct numerical simulation of turbulent boundary layers at Mach 3. *J. Fluid Mech.* **594**, 59–69.

Spalart, P. R. 1988 Direct simulation of a turbulent boundary layer up to $R_\theta = 1410$. *J. Fluid Mech.* **187**, 61–98.

Van Doorne, C. W. H. 2004 Stereoscopic PIV on transition in pipe flow. PhD thesis, Delft University of Technology.

https://doi.org/10.1017/S0022112010006336 Published online by Cambridge University Press